Influence of Hydrogen on the Structure of Amorphous Sputtered Fe–Co–Tb Films by Means of Wide- and Small Angle Neutron Scattering

M. Heckele, R. Bellissent[a], A. Brunsch[b], P. Lamparter, and S. Steeb

Max-Planck-Institut für Metallforschung, Institut für Werkstoffwissenschaft, 7000 Stuttgart, FRG

Z. Naturforsch. **46a**, 1015–1020 (1991); received October 12, 1991

Sputtered amorphous Fe–Co–Tb-films with perpendicular and in-plane magnetic anisotropy were investigated by wide- and small angle neutron scattering. By combination with X-ray data the maxima in the pair correlation function could be attributed to the individual atomic pairs. Thus also partial coordination numbers and a short range order parameter could be determined.

Wide angle diffraction revealed that the film with magnetic in-plane anisotropy contained 13 atomic percent hydrogen. The hydrogen incorporation causes substantial changes in the short range order, associated with enhanced formation of Tb-rich clusters, and the in-plane anisotropy. The clustering effect was confirmed by results from small angle scattering with polarized neutrons.

1. Introduction

Amorphous Fe–Co–Tb films are used as storage media in magneto-optic recording devices. Films are usually prepared by magnetron sputter processes and exhibit a magnetic easy axis perpendicular to the film plane, as required for storage applications, in a wide compositional range at least from 17 at.% up to 28 at.% Tb. It was already shown that the perpendicular magnetic anisotropy of vacuum deposited transition metal-rare earth films depends on the hydrogen content of the films [1, 2]. The influence of the H-contamination on the microstructure of Fe–Co–Tb was recently investigated by X-ray diffraction using the energy dispersive diffraction method (EDXD) [3]. In the present investigation the structural differences of a perpendicular anisotropic $Fe_{72}Co_8Tb_{20}$-film and an in-plane anisotropic $Fe_{68}Co_9Tb_{23}+H$-film are determined by wide- and small angle neutron scattering experiments. It has been shown [4] that the transition metal atoms Fe and Co can be mutually substituted isomorphously. Therefore in the following the two alloys are described as $TM_{80}Tb_{20}$ and $TM_{77}Tb_{23}$ with TM = Fe, Co (TM = transition metal).

[a] Laboratoire Léon Brillouin, Laboratoire Commun CEA-CNRS, 91191 Gif-sur-Yvette Cedex, France.

[b] IBM Germany, German Manufacturing Technology Center, 7032 Sindelfingen.

Reprint requests to Prof. Dr. S. Steeb, Institut für Werkstoffwissenschaft, Max-Planck-Institut für Metallforschung, Seestrasse 92, 7000 Stuttgart 1.

2. Theoretical

2.1 Wide Angle Scattering

Concerning the definitions of total structure factors $S(Q)$, with $Q = 4\pi \frac{(\sin \Theta)}{\lambda}$ = modulus of the scattering vector, 2Θ = scattering angle, and λ = wavelength of the radiation we refer to [5]. In that reference also the definitions of total pair correlation functions $G(R)$ and total pair distribution functions $g(R)$, with R = atomic distance in real space, are given together with the mathematical formalism according to which these functions follow from $S(Q)$.

A quantitative measure for the degree of chemical short range order is given by the refined Warren-Cowley short range order parameter $\alpha_{\text{ref.}}$ [6], which is obtained from the partial coordination numbers $Z_{\mu\nu}$:

$$\alpha_{\text{ref.}} = 1 - \frac{Z_{AB}\langle Z\rangle}{c_B Z_A Z_B}, \tag{1}$$

where

$$Z_A = Z_{AA} + Z_{AB},$$
$$Z_B = Z_{BA} + Z_{BB},$$
$$\langle Z\rangle = c_A Z_A + c_B Z_B.$$

For total segregation one has $\alpha_{\text{ref.}} = +1$, for compound formation $\alpha_{\text{ref.}} < 0$ with a minimum value of

$$\alpha_{\text{ref., min}} = \frac{c_A(Z_{AA}+Z_{AB})}{c_B(Z_{BA}+Z_{BB})} \leqq 1. \tag{2}$$

0932-0784 / 91 / 1200-1015 $ 01.30/0. – Please order a reprint rather than making your own copy.

Hereafter we use the normalized short range order parameter

$$\alpha_{\text{ref., norm.}} = \frac{\alpha_{\text{ref.}}}{\alpha_{\text{ref., min}}}. \tag{3}$$

2.2 Small Angle Scattering

An inhomogeneous system containing segregated uncorrelated particles (domains) yields a small angle scattering effect which converges at small Q-values into Guinier's law [7]:

$$I(Q) = I(0) \exp(-Q^2 R_G^2/3) \tag{4}$$

The Guinier-radius R_G can be evaluated from the slope of the straight line in a Guinier-plot ($\ln I(Q)$ vs. Q^2). If the particles are ball shaped the ball-diameter d_b can be obtained according to

$$d_b = 2 R_G \sqrt{\frac{5}{3}}. \tag{5}$$

2.2.1 Polarized Neutrons

Relative to an external magnetic field the magnetic moment of a primary neutron has two possible orientations (+) and (−). If one performs a diffraction experiment once with (+) and once with (−) polarized neutrons, then for the difference of the measured intensities we obtain

$$\Delta I = I^{(+)} - I^{(-)} \tag{6}$$

From such difference spectra one can deduce the correlation between atomic structure and magnetic moments in the specimen. Within the small angle region the intensity law is the following

$$I_{SA} \sim (\delta b + \delta p)^2 \tag{7}$$

with

δb = difference of the nuclear coherent scattering lengths of domains and matrix,

δp = difference of the magnetic coherent scattering lengths of domains and matrix.

The intensity difference is then:

$$\Delta I_{SA} \sim \delta b \cdot \delta p^{(+)} \tag{8}$$

with $\delta p^{(+)}$ = difference of the magnetic scattering lengths of domains and matrix for (+) polarized neutrons, and $p^{(+)} = -p^{(-)}$.

In the wide angle region the intensity scattered from the atomic pairs $\mu\nu$ amounts to

$$I_{WA}^{\mu\nu} \sim (b_\mu + p_\mu)(b_\nu + p_\nu) \tag{9}$$

and furthermore:

$$\Delta I_{WA}^{\mu\nu} \sim b_\mu p_\mu^{(+)} \left(\frac{p_\nu^{(+)}}{p_\mu^{(+)}} + \frac{b_\nu}{b_\mu} \right). \tag{10}$$

3. Experiments and Results

3.1 Sample Preparation

30 μm thick amorphous Fe–Co–Tb films were deposited onto both sides of 15 μm thick vanadium foils by rf magnetron sputtering. The starting pressure was 2×10^{-7} Torr and the film deposition was carried out in pure argon at a pressure of 10^{-2} Torr. For the neutron diffraction experiments 20 single films were stacked.

One specimen was prepared from films deposited from a composite $Fe_{72}Co_8Tb_{20}$ target, fabricated by vacuum casting. The second specimen was prepared from films deposited from a $Fe_{68}Co_9Tb_{23}$ target, fabricated by plasma-spraying in $(Ar + H_2)$ atmosphere.

The magnetic anisotropy of the films was measured with a vibrating sample magnetometer.

3.2 Wide Angle Scattering

The wide angle measurements were done at LLB-Saclay using the 7C2 Goniometer.

3.2.1 Intensity Curves

Figure 1 shows the intensity curves corrected for background and absorption as obtained with neutrons ($\lambda = 0.71$ Å) for the two amorphous alloys $TM_{77}Tb_{23}$ and $TM_{80}Tb_{20}$. In both cases a) and b) we observe a continuous decrease of the intensity with increasing Q, which shows a stronger Q-dependence with the upper curve. This could be identified as an incoherent contribution for the upper curve which is caused by hydrogen-impurities [4]. By means of a calibration procedure using a vanadium-standard we obtained a hydrogen content corresponding to $(TM_{0.77}Tb_{0.23})_{87}H_{13}$. The source of the hydrogen is the sputter target which was produced by plasma-spraying within an argon-hydrogen atmosphere.

The diffraction experiments were done at room temperature. Since the Curie-temperature for both

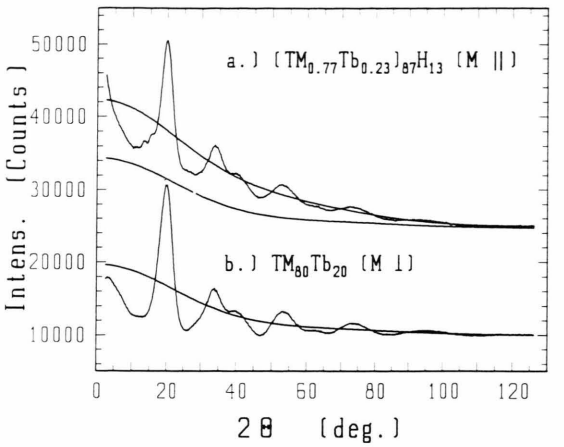

Fig. 1. Amorphous $(TM_{0.77}Tb_{0.23})_{87}H_{13}$ and amorphous $TM_{80}Tb_{20}$: Neutron diffraction ($\lambda = 0.71$ Å). Intensity corrected for background and absorption. a) Intensity curve containing scattering from hydrogen atoms and a magnetic incoherent contribution. The curve is shifted upwards. For comparison: magnetic contribution from curve b). b) Intensity curve containing a magnetic incoherent contribution.

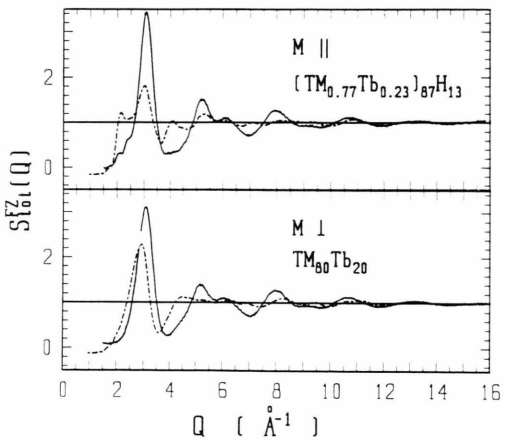

Fig. 2. Amorphous $(TM_{0.77}Tb_{0.23})_{87}H_{13}$ and amorphous $TM_{80}Tb_{20}$: Total structure factors according to Faber-Ziman;
—— neutron diffraction:
---- X-ray diffraction; (EDXD)-method [3].

specimens amounts to 150 °C, the intensity curves contain besides the incoherent magnetic scattering a coherent magnetic scattering contribution.

3.2.2 Total Structure Factors

The total Faber-Ziman structure factors obtained from the neutron diffraction experiments are plotted in Fig. 2 together with the EDXD-curves according to [3]. The two neutron structure factors are very similar. They show pronounced oscillations and a split up second maximum. The main peak of $(TM_{0.77}Tb_{0.23})_{87}H_{13}$ shows on its low-Q-side two small shoulders, whereas the $TM_{80}Tb_{20}$-curve increases monotonously within this region. The large differences between neutron- and X-ray-data can be explained on the basis of the weighting factors of the contributions of the partial structure factors to the total $S(Q)$ according to Faber-Ziman [8] which are listed in Table 1.

Table 1. Amorphous $(TM_{0.77}Tb_{0.23})_{87}H_{13}$ and amorphous $TM_{80}Tb_{20}$. Faber-Ziman X-ray (X) as well as neutron (n) weighting factors of the partial structure factors.

Specimen	$(TM_{0.77}Tb_{0.23})_{87}H_{13}$		$TM_{80}Tb_{20}$	
	X	n	X	n
W^{FZ}_{TM-TM}	0.31	0.72	0.39	0.69
W^{FZ}_{TM-Tb}	0.49	0.38	0.47	0.28
W^{FZ}_{Tb-Tb}	0.19	0.05	0.14	0.03
W^{FZ}_{TM-H}	0.00	−0.12	—	—
W^{FZ}_{Tb-H}	0.01	−0.03	—	—
W^{FZ}_{H-H}	0.00	0.00	—	—

Apparently, in the neutron experiments the TM–TM-correlations dominate. They are followed by the TM–Tb-correlations, whereas the Tb–Tb-correlations can be neglected. Concerning X-ray diffraction, the TM–Tb-correlations are weighted slightly stronger than the TM–TM-correlations and the Tb–Tb-weighting factor is about four times larger than in the neutron case. Caused by the large differences of the atomic diameters of TM and Tb the maxima of the different partial structure factors are shifted mutually in such a way that beyond the first maximum the X-ray intensity exhibits no pronounced oscillations. The peak at $Q = 2.13$ Å^{-1} in the X-ray structure factor of the $(TM_{0.77}Tb_{0.23})_{87}H_{13}$-specimen is in the neutron case only indicated as a small shoulder. This difference shows that it belongs to the Tb–Tb-correlation. Comparison with the $TM_{80}Tb_{20}$-curves points to a variation of this correlation upon hydrogen absorption.

3.2.3 Total Pair Correlation Functions

Figure 3 shows the total pair correlation functions as obtained with neutrons and compared with those obtained according to the EDXD-method. The neu-

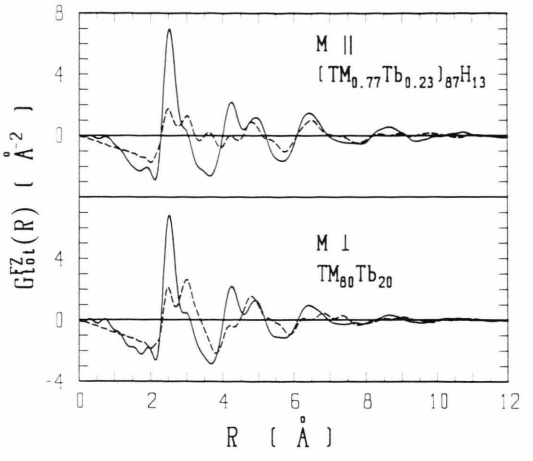

Fig. 3. Amorphous $(TM_{0.77}Tb_{0.23})_{87}H_{13}$ and amorphous $TM_{80}Tb_{20}$: Total pair correlation functions according to Faber-Ziman;
—— neutron diffraction:
---- X-ray diffraction; (EDXD)-method [3].

Table 2. Amorphous $(TM_{0.77}Tb_{0.23})_{87}H_{13}$ and amorphous $TM_{80}Tb_{20}$. Partial coordination numbers of the first [3] and second coordination sphere as well as the refined normalized Warren-Cowley short range order parameters $\alpha_{ref.,\,norm.}$

Specimen	Coordination numbers				
	Z_{TM-TM}	Z_{TM-Tb}	Z_{Tb-TM}	Z_{Tb-Tb}	$\alpha_{ref.,\,norm.}$
1. Coordination sphere					
$(TM_{0.77}Tb_{0.23})_{87}H_{13}$	8.8	2.6	8.6	7.0	+0.22
$TM_{80}Tb_{20}$	6.6	3.3	13.2	3.5	−0.29
2. Coordination sphere					
$(TM_{0.77}Tb_{0.23})_{87}H_{13}$	12.1	8.4	28.1	14.0	−0.13
$TM_{80}Tb_{20}$	7.6	9.1	36.4	26.3	−0.13

tron curves are determined strongly by the TM–TM-correlations, whereas the X-ray curves also show pronounced contributions of the TM–TM-, TM–Tb-, and Tb–Tb-correlations. The nearest neighbour pairs can be identified from the EDXD-curves alone on the basis of the atomic diameters of TM and Tb, those of the more distant coordination shells by combination of the X-ray- and neutron curves.

For example, if an X-ray- and a strong neutron-maximum coincide, then these maxima belong to a TM–TM-correlation. Are the X-ray- and the neutron-maxima of the same height, then they will be caused by a TM–Tb-correlation. If the neutron curve shows no peak at the corresponding position of an X-ray peak, then this is a hint on a Tb–Tb-correlations. In this way for both kinds of specimens the identification of the pairs within the first coordination shell as deduced from the EDXD-$G_{tot}(R)$ can be proved by the neutron data.

Concerning the second coordination sphere for 3.8 Å $\leqq R \leqq$ 5.9 Å the following can be stated. The peak at $R = 4.24$ Å belongs to a TM–TM-correlation and the peak at 4.94 Å to a TM–Tb-correlation whereas the shoulder at 5.4 Å in the X-ray curve belongs to a Tb–Tb-correlation.

In the third coordination sphere (5.9 Å $\leqq R \leqq$ 8 Å) slight differences occur between the two specimens. For $TM_{80}Tb_{20}$ the TM–TM-correlation at 6.3 Å and the TM–Tb-correlation at 6.8 Å are separated in the EDXD-correlation function. For $(TM_{0.77}Tb_{0.23})_{87}H_{13}$ only a broad maximum at 6.5 Å can be observed. Both specimens show a Tb–Tb-correlation at 7.3 Å.

Since in the second coordination sphere the peaks can be assigned to the specific correlations it is also possible to determine the partial coordination numbers. This was done by fitting Gaussians to the peaks of the EDXD-$[(G(R)/4\pi R\varrho_0)+1]$ (ϱ_0 = number density). From the partial coordination numbers the normalized refined Warren-Cowley short range order parameter $\alpha_{ref.,\,norm.}$ was calculated. These values together with the partial coordination numbers are compiled in Table 2.

For the first coordination sphere of amorphous $(TM_{0.77}Tb_{0.23})_{87}H_{13}$ Utz et al. [3] found $\alpha_{ref.,\,norm.} = +0.22$, i.e. segregation tendency, which up to that time never was reported for amorphous alloys. Thereby only the partial coordination numbers of the subsystem $TM_{77}Tb_{23}$ were considered. The amorphous $TM_{80}Tb_{20}$ alloy shows compound forming tendency. Apparently, the structural differences between the two specimens are caused by the hydrogen atoms which, according to the chemical affinity will prefer sites near Tb-atoms. This is also indicated by the rather strong variation of the X-ray intensity curves when hydrogen is embedded. The Tb–Tb coordination number in the first coordination sphere is twice as large for the hydrogen-containing specimen than for the $TM_{80}Tb_{20}$ specimen. Obviously the hydrogen-terbium interaction causes a clustering of the Tb-atoms. This increase of the number of Tb–Tb pairs implies decrease in the number of TM–Tb pairs and thus an increase in the number of TM–TM-pairs.

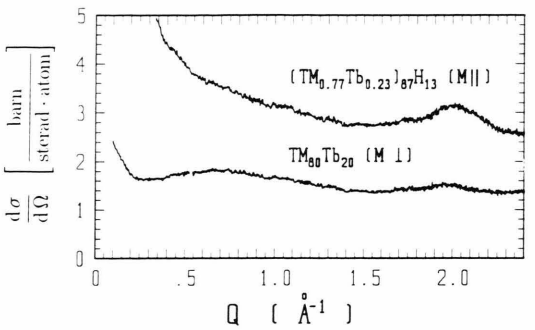

Fig. 4. Amorphous $(TM_{0.77}Tb_{0.23})_{87}H_{13}$and amorphous $TM_{80}Tb_{20}$: Neutron diffraction; differential scattering cross section.

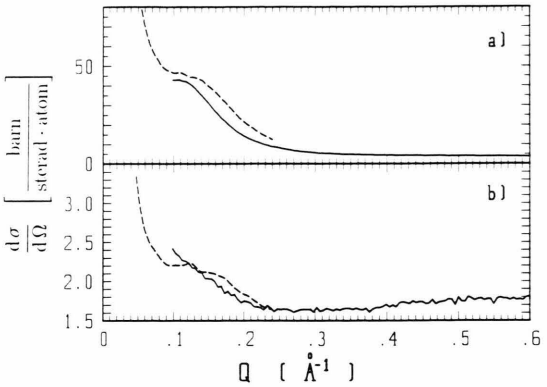

Fig. 5. a) Amorphous $(TM_{0.77}Tb_{0.23})_{87}H_{13}$; b) Amorphous $TM_{80}Tb_{20}$.
—— Neutron diffraction, differential scattering cross section;
---- X-ray diffraction in arbitrary units.

3.3 Small Angle Scattering

The measurements were done at the Saclay instrument G6-1 using cold neutrons ($\lambda = 4.721$ Å) where the range of scattering angle $4.3° \leqq 2\Theta \leqq 129°$ corresponds to a Q-range $0.1\ \text{Å}^{-1} \leqq Q \leqq 2.4\ \text{Å}^{-1}$, which has an overlap with the wide angle measurements.

3.3.1 Unpolarized Neutrons

Figure 4 shows the differential scattering cross sections for the two amorphous specimens $(TM_{0.77}Tb_{0.23})_{87}H_{13}$ and $TM_{80}Tb_{20}$. The first one shows a rather strong increase towards small-Q-values, whereas with $TM_{80}Tb_{20}$ the increase is smaller and also the scattered intensity at all. With $TM_{80}Tb_{20}$ a maximum occurs at $Q = 0.7\ \text{Å}^{-1}$ which belongs to an atomic distance of 11 Å if regarded as the first maximum of a $\frac{\sin QR}{QR}$-curve. At $2\ \text{Å}^{-1}$ we observe a small peak in Fig. 4 which was not visible in Fig. 2 because of the worse resolution. With the hydrogen-containing sample the peak at $Q = 2\ \text{Å}^{-1}$ is higher and was indicated in Fig. 2 as obtained using the wide angle goniometer 7C2.

Figure 5 shows the scattering cross sections of the two specimens in the region $0 \leqq Q \leqq 0.6\ \text{Å}^{-1}$. This figure contains besides the neutron curves also the X-ray results. With the hydrogenated sample (Fig. 5a) both curves show a plateau at $Q = 0.12\ \text{Å}^{-1}$ which for amorphous $TM_{80}Tb_{20}$ in Fig. 5b only occurs in the X-ray curve.

From the fact that the small angle signal is also observed with X-rays we conclude that the corresponding inhomogeneities are compositional and not merely magnetic.

From a Guinier plot of the intensity in the range $0.1\ \text{Å}^{-1} \leqq Q \leqq 0.2\ \text{Å}^{-1}$ for $TM_{80}Tb_{20}$ a diameter $d_b = 14$ Å, and in the range $0.14\ \text{Å}^{-1} \leqq Q \leqq 0.2\ \text{Å}^{-1}$ for $(TM_{0.77}Tb_{0.23})_{87}H_{13}$ a diameter $d_b = 30$ Å was obtained.

Thus the storage of hydrogen leads to an enlargement of the diameter of segregated regions by a factor of two. Most probably these regions are enriched in Tb. Loading with hydrogen enhances the clustering of the Tb atoms. This view is supported by the increase of the coordination number Z_{TbTb} as deduced from the wide angle scattering experiments. The cluster formation from Tb and H finally has the consequence that the magnetic easy axis switches from perpendicular to in-plane.

3.3.2 Polarized Neutrons

Figure 6 shows the difference intensity curves $\Delta \frac{d\sigma}{d\Omega}(Q)$ in dependence of an external magnetic field applied parallel to the specimen plane and perpendicular to the direction of the scattering vector Q.

For both specimens the difference spectra in Fig. 6 change at $Q = 1.8\ \text{Å}^{-1}$ from positive to negative sign. This behaviour is discussed in the following.

With amorphous $(TM_{0.77}Tb_{0.23})_{87}H_{13}$ the small angle scattering is caused by Tb-rich clusters. Under the assumption that the number densities of the matrix and the clusters are the same it can be shown that the differences of the scattering lengths of the matrix and the domains in (8) can be replaced by the differences of the scattering lengths of the two atomic spe-

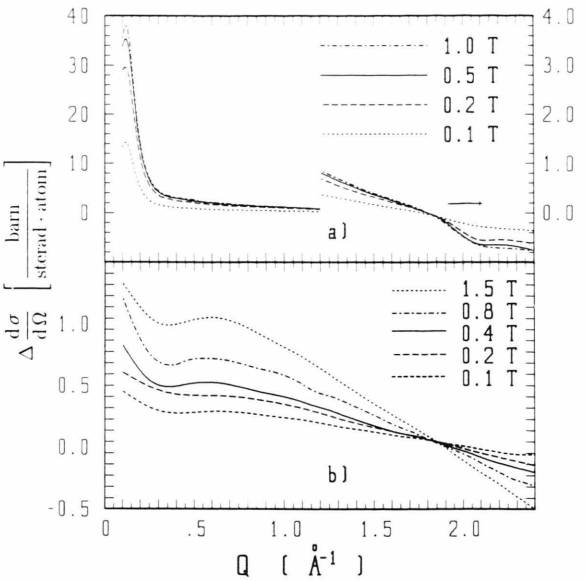

Fig. 6. Neutron diffraction using polarized neutrons: Difference spectra $\frac{d\sigma^{(+)}}{d\Omega} - \frac{d\sigma^{(-)}}{d\Omega}$ in dependence from the external magnetic field, a) Amorphous $(TM_{0.77}Tb_{0.23})_{87}H_{13}$; b) Amorphous $TM_{80}Tb_{20}$.

cies. Then (8) becomes

$$\Delta\frac{d\sigma}{d\Omega} \sim (b_{Tb} - b_{TM})(p_{Tb}^{(+)} - p_{TM}^{+}) = \Delta b \cdot \Delta p. \quad (11)$$

Regarding the iron- and cobalt-concentration one obtains the scattering length $b_{TM} = 0.913 \cdot 10^{-12}$ cm. With $b_{Tb} = 0.738 \cdot 10^{-12}$ cm, we obtain $\Delta b < 0$. $TM_{77}Tb_{23}$ is ferrimagnetic, i.e. the magnetic moments of the Tb- and the TM-atoms are antiparallel. According to the application of those alloys as magneto-optic storage media the composition was chosen in such a way that the resulting magnetization of the specimen at room temperature is close to zero, and thus:

$$c_{TM}\, p_{TM}^{(+)} + c_{Tb}\, p_{Tb}^{(+)} = 0. \quad (12)$$

Therefore

$$\Delta p = p_{Tb}^{(+)} - p_{TM}^{(+)} = p_{Tb}^{(+)}\left(1 - \frac{c_{Tb}}{c_{TM}}\right). \quad (13)$$

Because the difference signal $\Delta\frac{d\sigma}{d\Omega}$ is positive and Δb negative, the contribution of $p_{Tb}^{(+)}$ is negative.

Based on this we can discuss now the negative run of the difference spectra for $Q \geqq 1.8$ Å^{-1} using (10):

With $p_{Tb}/p_{Fe} \approx 4$ it can be shown that Tb–Tb as well as Tb–Fe pairs yield a negative contribution to $\Delta\frac{d\sigma}{d\Omega}$ according to (10). In connection with the explanation of the peak at 2.13 Å^{-1} in the $(TM_{0.77}Tb_{0.23})_{87}H_{13}$-structure factor as a contribution from Tb–Tb correlations, it is suggested that the negative difference signal $\Delta\frac{d\sigma}{d\Omega}$ at $Q > 1.8$ Å^{-1} is due to Tb–Tb pairs.

Concerning the dependence of the difference spectra from the applied external magnetic field we observe in Fig. 6 that $\Delta\frac{d\sigma}{d\Omega}$ increases with increasing magnetic field. In Fig. 6a there is a saturation effect with increasing field. In Fig. 6b the increase is far from a saturation at the maximum field of 1.5 T.

For the amorphous $(TM_{0.77}Tb_{0.23})_{87}H_{13}$-specimen the direction of the magnetic easy axis is already in the film plane and an external magnetic field of 1 T is sufficient to orientate the magnetic domains.

The amorphous $TM_{80}Tb_{20}$-specimen exhibits a strong perpendicular anisotropy. Therefore the applied fields are not strong enough to saturate the film.

[1] A. Brunsch and J. Schneider, IEEE Trans. Mag., MAG-14, No. 5, Sept. 1978, p. 731 ff.
[2] T. Niihara, S. Takayama, and Y. Sugita, IEEE Trans. Mag., MAG-21, Nr. 5, Sept. 1985, p. 1638 ff.
[3] R. Utz, A. Brunsch, P. Lamparter, and S. Steeb, Z. Naturforschung **44a**, 1201 (1989).
[4] M. Heckele, Doctor Thesis, University of Stuttgart, 1991.
[5] S. Steeb, S. Falch, and P. Lamparter, Z. Metallkde. **75**, 599 (1984).
[6] S. Steeb and P. Lamparter, Proc. Int. Conf. Order-Disorder, Grenoble, 1991; Elsevier Science Publishers, Editor A. R. Yavari, 1992.
[7] A. Guinier and G. Fournet, Small Angle Scattering of X-Rays, John Wiley & Sons Inc., London, 1955.
[8] T. E. Faber and J. M. Ziman, Phil. Mag., **11**, 153 (1965).